Glass-Ceramic Sodium-Deficient Chlorides with High Sodium-ion Conductivity

Phillip Ridley[a], Long Hoang Bao Nguyen[a], Elias Sebti[b], George Duong[a], Yu-Ting Chen[c], Baharak Sayahpour[c], Ashley Cronk[c], Grayson Deysher[c], So-Yeon Ham[c], Jin An Sam Oh[a], Erik A. Wu[a], Darren H. S. Tan[a], Jean-Marie Doux[a], Raphaële Clément[b], Jihyun Jang[a,*], Ying Shirley Meng[a,d,*]

[a]*Department of NanoEngineering, University of California, San Diego, La Jolla 92093, CA, United States*
[b]*Department of Materials, University of California, Santa Barbara, Santa Barbara, CA 93117, United States*
[c]*Materials Science and Engineering Program, University of California San Diego, La Jolla 92093, CA, United States*
[d]*Pritzker School of Molecular Engineering, The University of Chicago, Chicago, IL 60637, United States*

*Corresponding author. Email: jijang@eng.ucsd.edu
*Corresponding author. Email: shirleymeng@uchicago.edu

Abstract

Solid-state batteries are a promising energy storage technology that can potentially offer both improved safety and energy density. The solid electrolyte is the defining feature and plays a significant role in the electrochemical performance of a solid-state cell, especially at room temperature. Herein, we report a series of glass-ceramic, sodium-deficient chloride solid electrolytes, $Na_xY_{0.25}Zr_{0.75}Cl_{3.75+x}$ ($0.25 \leq x \leq 0.875$), possessing significantly improved ionic conductivities when compared to their stoichiometric counterpart, $Na_{2.25}Y_{0.25}Zr_{0.75}Cl_6$ ($x = 2.25$). By tuning both the sodium molar content and the sample's crystallinity, the composition $Na_{0.625}Y_{0.25}Zr_{0.75}Cl_{4.375}$ ($x = 0.625$) was found to exhibit the highest Na^+ conductivity of 0.4 mS cm^{-1} at room temperature. Furthermore, the relationship between composition, structure, and conductivity for these compositions in the $NaCl{-}YCl_3{-}ZrCl_4$ system was evaluated using a combination of X-ray diffraction (XRD), solid-state nuclear magnetic resonance spectroscopy (ss-NMR), and electrochemical impedance spectroscopy (EIS) techniques. Materials characterization reveals that sodium-deficiency (i.e., lower molar % of NaCl) results in reduced crystallinity and preferred occupancy of prismatic Na local environments. These combined factors contribute to a lower activation energy for Na^+ hopping, an increased ionic conductivity, and improved electrochemical performance at both higher cycling rates and at room temperature.

Main

As society trends toward renewable energy sources, there is an undoubted need to implement energy storage devices that can both electrify transportation and complement intermittent power sources, like wind and solar. All-solid-state batteries (ASSBs) have emerged as a promising pathway forward, which can address the anticipated gap in energy storage capacity by theoretically providing much larger energy densities. When considering grid-level energy storage, a sustainable supply of ASSB materials must be realized and a low cost per kilowatt-hour is necessary. As such, sodium ASSBs are a prospective technology for these large-scale applications, owed to the usage of intrinsically cheaper and more abundant raw materials.[1–3] Moreover, sodium ASSBs have been shown to deliver stable long-term cycling, possibly enabling both a long battery lifetime and lower overall cost.[4]

Solid electrolytes (SEs) are the cornerstone of ASSBs, ultimately playing a principal role in the device's performance. Inorganic SEs are a group of materials that can exhibit superionic conductivities at ambient temperature in both lithium- and sodium-based systems, some of which possess conductivities comparable to or even surpass those of liquid-organic electrolytes.[5] Previously, ceramic and glass-ceramic materials, like NASICON-type oxide phases, Na_3PS_4 (NPS), and $Na_{2.88}Sb_{0.86}W_{0.11}S_4$ sulfides, have exhibited some of the highest Na^+ conductivities.[6–10] However, due to the high interfacial resistance between oxide SEs and active material particles, additional high-temperature sintering steps are necessary to achieve adequate interfacial contact and nullify contact resistance.[11] Consequently, sulfide SEs have attracted a lot of attention due to their high ionic conductivities, while also exhibiting lower bulk moduli and thus better deformability under applied pressure at room temperature.[12] This favorable deformability leads to lower porosity and creates more contact points between active materials and the SE.

Despite better processability, sulfides suffer from narrow electrochemical stability windows, which can lead to severe interfacial degradation reactions during cycling, yielding high interfacial resistance and inducing eventual cell failure.[13] Nevertheless, while protective coatings have been implemented to prevent side reactions between the cathode and SEs, the oxidation of sulfide SEs under high voltage still occurs and results in poor electrochemical performance.[14,15] Recently, it was shown that a bilayer electrolyte cell design utilizing NPS as the separator layer and a chloride-based catholyte in the cathode composite, can completely avoid interfacial side reactions between

NPS and the active material, thus delivering stable long-term cycling.[4] Therefore, developing a highly conductive SE or catholyte material that is stable over a wide range of potentials is essential for ASSB development. Such a material can enable the use of high-voltage cathode materials and improve long-term cyclability without the need for protective coating layers.

Within the past five years, chlorides SEs have emerged as promising catholytes, offering excellent electrochemical stability at high voltages, high ionic conductivity, and good cyclability when paired with suitable oxide cathode materials.[4,16–21] In 2018, Asano *et al*. first reported the mechanochemical synthesis of Li_3YCl_6 (LYC), which exhibited a high ionic conductivity of ~ 0.5 mS cm^{-1}.[16] Interestingly, it was shown that the ionic conductivity of LYC decreased with an increased crystallinity of the phase. In the same work, it was proposed that the Y^{3+} cations in LYC occupy octahedral sites that are alternatively stacked along the *c*-direction, which can partially block Li^+ diffusion. However, low crystalline (lc-) LYC possessing Y^{3+} anti-site defects was generated via ball milling, leading to poorer crystallinity and improved ionic conductivity.[16] Sebti *et al.* showed that, rather than random disorder on the Y lattice, Y layer stacking faults in LYC are formed during ball milling and drastically lower Li^+ diffusion barriers through the structure, thus increasing intragrain transport.[22]

Besides crystallinity, the concentration of vacancies also plays an important role in the resultant ionic conductivity. Aliovalent substitutions have been implemented to create additional vacancies that enhance ionic transport.[4,23] Recently, Liang *et al*. explored the concept of Li-deficiency in chloride-based Li_xScCl_{3+x} ($0 \leq x \leq 4$) SEs, where the authors showed that Li^+ conductivity and activation energy vary significantly depending on the ratio of LiCl to $ScCl_3$ used during synthesis.[24] Although the accurate structure of these Li_xScCl_{3+x} phases remain unclear, the concept is still promising as it can enhance the materials' ionic conductivity without the incorporation of another transition metal. To the best of our knowledge, this concept has never been explored for chloride-based Na^+ conductors.

Sodium chloride-based materials, primarily of the Na_3MCl_6 and Na_2MCl_6 compositions (M^{3+} = Y^{3+}, Er^{3+}, Gd^{3+} and M^{4+} = Zr^{4+}), have emerged as promising catholytes for Na-ASSBs.[25–28] Mechanochemical syntheses of Na_3YCl_6, Na_3ErCl_6, and Na_2ZrCl_6 have all yielded relatively low Na^+ conductivities ($\leq 10^{-5}$ S cm^{-1}) and have thus required the implementation of aliovalent substitution. Consequently, the syntheses of $Na_{3-y}Y_{1-y}Zr_yCl_6$ ($0 \leq y \leq 1$) solid solutions were recently reported, whose maximum ionic conductivity was observed at the $y = 0.75$ composition.[4]

This increased ionic conductivity was attributed to the introduction of Na vacancies, an optimal unit cell volume, and cooperative MCl_6 rotation.[4,29] Moreover, it was observed that the ionic conductivity of the $y = 0.75$ composition was lower after crystallization from heat treatment and reached its highest value after amorphization as result of ball milling, further demonstrating this relationship between crystallinity and ionic conductivity in chloride-based SEs. Therefore, the design of Na-chloride SEs should be focused on optimizing crystallinity and the concentration of Na vacancies to promote more favorable Na^+ diffusion.

In this study, we investigate the synergistic effects of crystallinity and Na-deficiency on the ionic conductivity of $Na_{3-y}Y_{1-y}Zr_yCl_6$ SEs. To minimize the total number of variables, the Y:Zr ratio was fixed at 1:3, corresponding to the highest ionic conductivity previously observed in the $Na_{3-y}Y_{1-y}Zr_yCl_6$ series. The NaCl molar % was varied, leading to a compositional series of Na-deficient samples, $Na_xY_{0.25}Zr_{0.75}Cl_{3.75+x}$ ($0.25 \leq x \leq 0.875$). The possible variables and factors which can affect the ionic conductivity of the SEs studied in this work are highlighted in **Figure 1a**. Our results reveal that Na-deficiency, along with low crystallinity, help to increase the ionic conductivity of the samples when compared to the stoichiometric composition, $Na_{2.25}Y_{0.25}Zr_{0.75}Cl_6$ (NYZC-2.25), which is not Na-deficient. The enhanced ionic conductivity is attributed to synergistic effects between low crystallinity, Na^+ vacancies, and prismatic Na local environments, all of which serve to improve the performance of ASSBs, especially at high cycling rates and at room temperature.

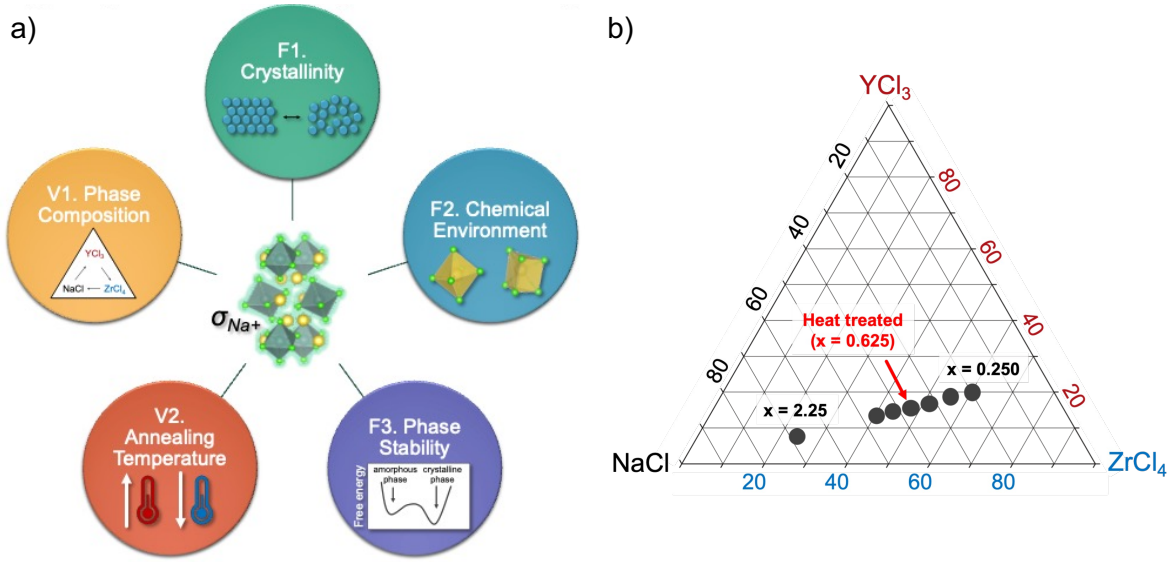

Figure 1. a) Variables (V) and factors (F) that can affect the ionic conductivity of the $Na_xY_{0.25}Zr_{0.75}Cl_{3.75+x}$ ($0.25 \leq x \leq 0.875$) SEs investigated in this work. b) Ternary phase diagram between NaCl–YCl_3–$ZrCl_4$ precursors, illustrating the molar ratios explored in this work.

Structural Analysis and Ionic Conductivity Measurements. Figure 1b. shows the NaCl–YCl_3–$ZrCl_4$ ternary phase diagram, where the highlighted points illustrate the molar ratios explored in this work, e.g., $Na_xY_{0.25}Zr_{0.75}Cl_{3.75+x}$ ($0.25 \leq x \leq 0.875$) or Na_xYZC_x. The X-ray diffraction (XRD) patterns show that few and low-intensity Bragg reflections were observed in all samples (**Figure 2a**). Moreover, no significant signals from the Bragg peaks of NaCl, YCl_3, or $ZrCl_4$ were observed after the ball-milling process, except for a small amount of unreacted NaCl precursor detected when $x > 0.5$ in Na_xYZC_x. Furthermore, all the diffraction peaks were broad indicating a low crystallinity or an amorphous state of the synthesized products. As the molar ratio of NaCl was decreased from $x = 0.875$ to $x = 0.25$, a broadening of the major reflection at $2\theta \sim 7.2°$ is clearly observed. This can be an indication of a reduction in the average crystallite domain size and thus a lower crystallinity. To quantify the degree of crystallinity of the samples, the full width at half maximum (FWHM) of the main reflection at $2\theta \sim 7.2°$ was used to estimate the average domain size of the crystallites according to Scherrer's equation (Equation 1):

$$\tau = \frac{K\lambda}{\beta \cos\theta} \qquad \text{Equation (1)}$$

where τ is the mean size of the coherent domain, K is the shape factor, λ is the X-ray radiation wavelength, β is the FWHM of the peak of interest, and θ is the Bragg angle.

Figure 2b shows that when the NaCl content was reduced from $x = 0.875$ to $x = 0.625$, the average domain size decreases from ~ 6 to ~ 3 nm. The molar content of NaCl is directly correlated to the crystallinity of the phase, where lowering NaCl amounts lead to lower crystallinity. At the composition where the molar content of NaCl is lowest ($x = 0.25$), Bragg peaks are essentially non-existent and the main reflection is significantly broadened, indicating that the obtained phase is highly disordered and lacks any significant long-range order (**Figure 2a**).

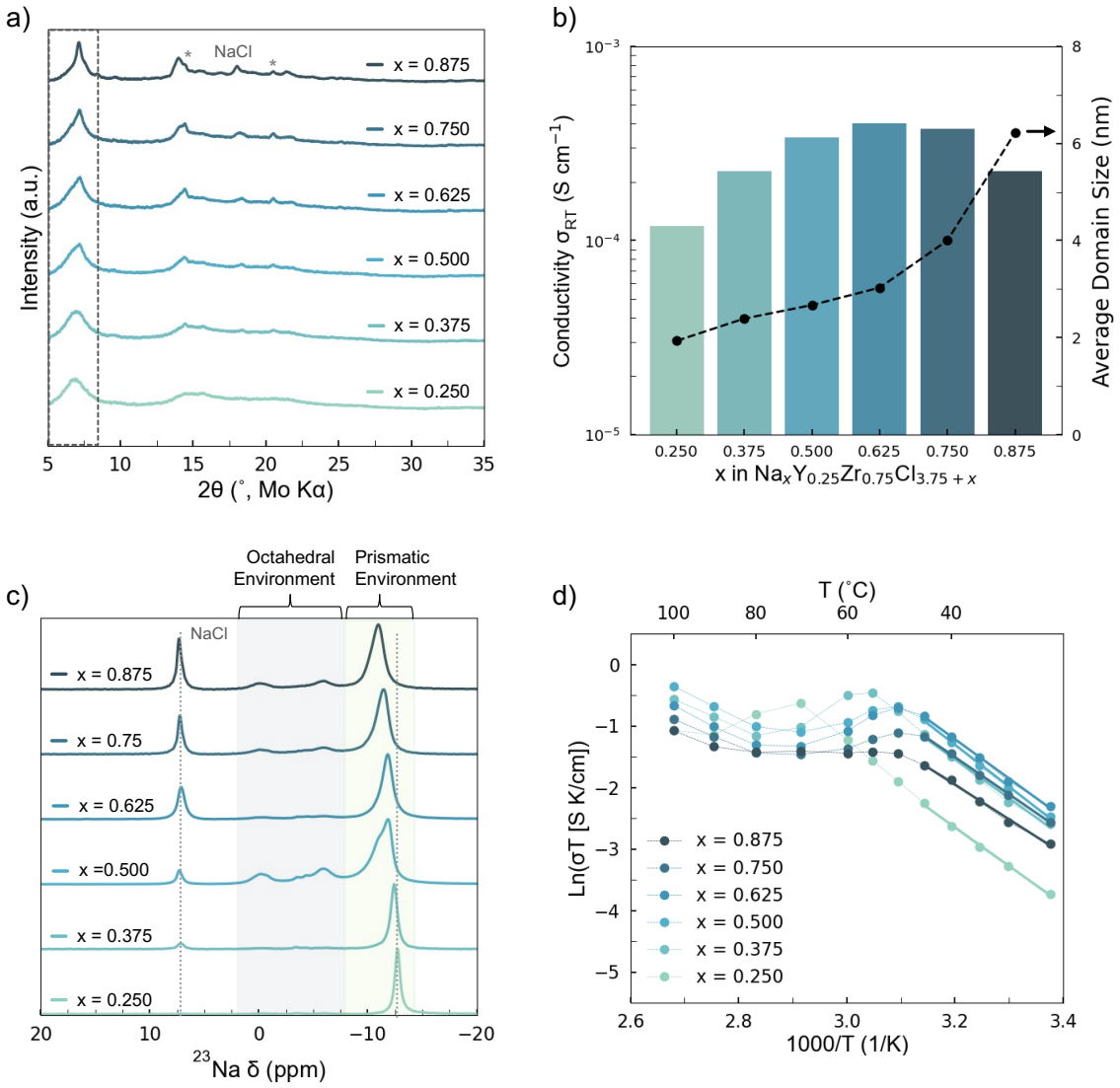

Figure 2. a) XRD patterns of $Na_xY_{0.25}Zr_{0.75}Cl_{3.75+x}$ (x = 0.875, 0.75, 0.625, 0.5, 0.375, and 0.25) compositions. Bragg peaks corresponding to unreacted NaCl are marked with asterisks. Dashed lines indicate the Bragg feature used for estimating crystallite size. b) Room temperature (~ 22 ºC) conductivity measurements for $Na_xY_{0.25}Zr_{0.75}Cl_{3.75+x}$ ($0.25 \leq x \leq 0.875$) compositional series. c) ^{23}Na ss-NMR spectra recorded on $Na_xY_{0.25}Zr_{0.75}Cl_{3.75+x}$ (x = 0.875, 0.75, 0.625, 0.5, 0.375, and 0.25) compositions. d) Arrhenius plot for $Na_xY_{0.25}Zr_{0.75}Cl_{3.75+x}$ compositional series.

Due to the low crystallinity of the $Na_xY_{0.25}Zr_{0.75}Cl_{3.75+x}$ ($0.25 \leq x \leq 0.875$) compositional series, the local Na environments were investigated using ^{23}Na solid-state nuclear magnetic resonance (ss-NMR) spectroscopy. Room temperature ^{23}Na ss-NMR spectra were acquired on all Na_xYZC_x

compositions and are presented in **Figure 2c**. The peak located around 7.2 ppm, which is observed in all samples, can be attributed to minor amounts of unreacted NaCl precursor.[4,30] As the molar ratio of NaCl decreases, there is a corresponding reduction in NaCl signal, which is in good agreement with the XRD results. The two weak and broad signals detected in the range of -2.5 − 8 ppm are attributed to octahedral Na environments, while the intense resonance around -10 to -13 ppm is attributed to prismatic Na environments, both of which are assigned according to the recently reported local structure of the crystalline analogue.[31] Interestingly, the prismatic signal can be clearly observed even at very low NaCl molar percentages, while the signals corresponding to octahedral environments can only be detected when $x > 0.5$. This observation reveals that Na^+ cations preferentially occupy prismatic environments, which is similar to what has been reported in some Na-based layered oxides and other chloride SEs.[23,32] Additionally, the resonance of the prismatic environment narrows significantly when $x < 0.5$, indicating a likely increase in the mobility of Na^+ at lower NaCl molar percentages.

Figure 2b shows the ionic conductivities measured at room temperature (~ 22 °C) for all the Na_xYZC_x compositions. The Nyquist plots corresponding to the raw data are shown in **Figure S1a.** All SE samples exhibited high Na^+ conductivities (> 1.0×10^{-4} S cm^{-1}), with a maximum value of 4.0×10^{-4} S cm^{-1} at the $x = 0.625$ composition. These values are all significantly higher than what has been previously reported for the stoichiometric $Na_{2.25}Y_{0.25}Zr_{0.75}Cl_6$ (6.6×10^{-5} S cm^{-1}) phase.[4] Interestingly, the sample with the lowest mol % of NaCl ($x = 0.25$) still exhibited an ionic conductivity comparable to NPS and is still higher than all other previously reported chloride-based Na^+ SEs.[4,23,28,33]

The ionic conductivity of a single ion conductor is determined by the relation:

$$\sigma = n_i q_i \mu_{\mathrm{i}} \qquad \text{Equation (2)}$$

where σ is the ionic conductivity, n_i is the number of charge carriers of species i, q_i is the charge of species i, and μ_i is the mobility of species i.

Glassy or amorphous SEs usually possess lower densities than their crystalline counterparts, allowing for the presence of additional free volume which is attributed to their non-periodicity and lower packing densities.[34] Moreover, free volume has been shown to promote more favorable ionic diffusion and thus enhanced ionic conductivity.[35,36] Here, it can be speculated that the low crystalline Na_xYZC_x compositions should possess higher free volume compared to the stoichiometric $Na_{2.25}Y_{0.25}Zr_{0.75}Cl_6$ system, which may contribute to the improved Na^+ mobility.

Moreover, since the total conductivity is a product of n_{Na} and μ_{Na}, an optimum balance between the two is expected to achieve the highest conductivity. On one hand, there will not be enough charge carriers when the concentration of Na^+ is too low. Conversely, the number of vacancies and free volume will be significantly reduced at higher NaCl molar percentages, resulting in lower Na^+ mobility. As such, $Na_{0.625}Y_{0.25}Zr_{0.75}Cl_{4.375}$ (NYZC-0.625) appears to be the optimal composition due to a balancing between the available volume free and the concentration of mobile Na^+ cations. The Arrhenius plots of all Na_xYZC_x compositions show that ln(σT) versus $f(1/T)$ evolves linearly at temperatures below ~50 °C (**Figure 2d**) and the activation energy for Na^+ diffusion can then be extracted using the Arrhenius equation:

$$\sigma = \frac{\sigma_0}{T} e^{-\frac{E_a}{k_B T}} \qquad \text{Equation (3)}$$

where σ_o is the Arrhenius pre-factor, E_a is the activation energy, and k_B is the Boltzmann constant.

All Na_xYZC_x compositions possessed activation energies in the range of 480 − 540 meV (**Table S1**), which are all appreciably lower than the stoichiometric $Na_{2.25}Y_{0.25}Zr_{0.75}Cl_6$ (664 meV) phase.[4] Surprisingly, all of the Na_xYZC_x compositions deviated from this ln(σT) $\propto$ 1/T linear relationship at temperatures above ~50 °C (**Figure 2d**). This deviation from linearity was accompanied by a drop in the sample's ionic conductivity and a return to linear ln(σT) $\propto$ 1/T behavior at higher temperatures. The temperature at which these deviations occur appears to vary with the composition and the crystallinity of the sample, where a higher transition temperature was observed for lower NaCl molar percentages (**Figure 2d** and **Table S1**).

Non-linear Arrhenius Behavior. To better understand the non-linear Arrhenius behavior, the optimal composition with the highest ionic conductivity, NYZC-0.625, was selected for further study. The sample was heat-treated at different temperatures (50, 60, 70, and 100 °C), and the measured ionic conductivities and activation energies of the recovered powders are reported in **Figure 3a** and **Table S2**, respectively. Samples which were subjected to higher heat treatment temperatures exhibited lower ionic conductivities and increased activation energies, which agrees well with many other chloride SEs reported in the literature.[4,16,28] Notably, the Arrhenius plot of the samples heated at 50, 60, and 70 °C still exhibited non-linear behavior at elevated temperatures. However, the temperature where the deviation occurred shifted to higher values compared to the

as-milled sample. Surprisingly, the sample treated at 100 °C showed a linear $\ln(\sigma T) \propto 1/T$ relationship throughout the whole temperature range (**Figure 3a**), indicating a significant change in the sample's structure due to the heat treatment step.

XRD patterns of the NYZC-0.625 powders recovered after the various thermal treatments are shown in **Figure 3b**. Upon heating, all diffraction peaks appeared to become narrower, providing evidence of a crystallization process. The average size of the coherent domains, determined again from the diffraction peak at 7.2°, grew gradually until reaching a maximum value of ~ 12 nm at 100 °C and was accompanied by drops in the ionic conductivity (**Figure 3c**). The corresponding ^{23}Na ss-NMR spectra show that more NaCl was consumed and incorporated into the main structure when the sample was subjected to heating at higher temperatures (**Figure 3d**). Furthermore, the resonance corresponding to prismatic Na sites decreased while those of octahedral Na environments grew significantly. Therefore, higher heat treatment temperatures promote crystallization of the phase, accompanied by a preferential population of octahedral over prismatic Na sites. A simple geometry comparison between the two polyhedral reveals that the cross-sectional areas of prismatic $[NaCl_6]^{5-}$, in which Na ions diffuse through, is significantly larger than those of octahedral $[NaCl_6]^{5-}$ (**Figure 3e**). As such, is it hypothesized that the Na^+ hopping between prismatic sites requires lower activation energy, thus leading to more favorable Na diffusion. Previous studies on P2-type layered manganese oxides have also reported fast Na^+ self-diffusion via edge- and face-sharing prismatic Na sites.[32] The preferential population of prismatic environments is likely one of the factors aiding the Na-deficient compositions Na_xYZC_x to achieve enhanced ionic conductivity.

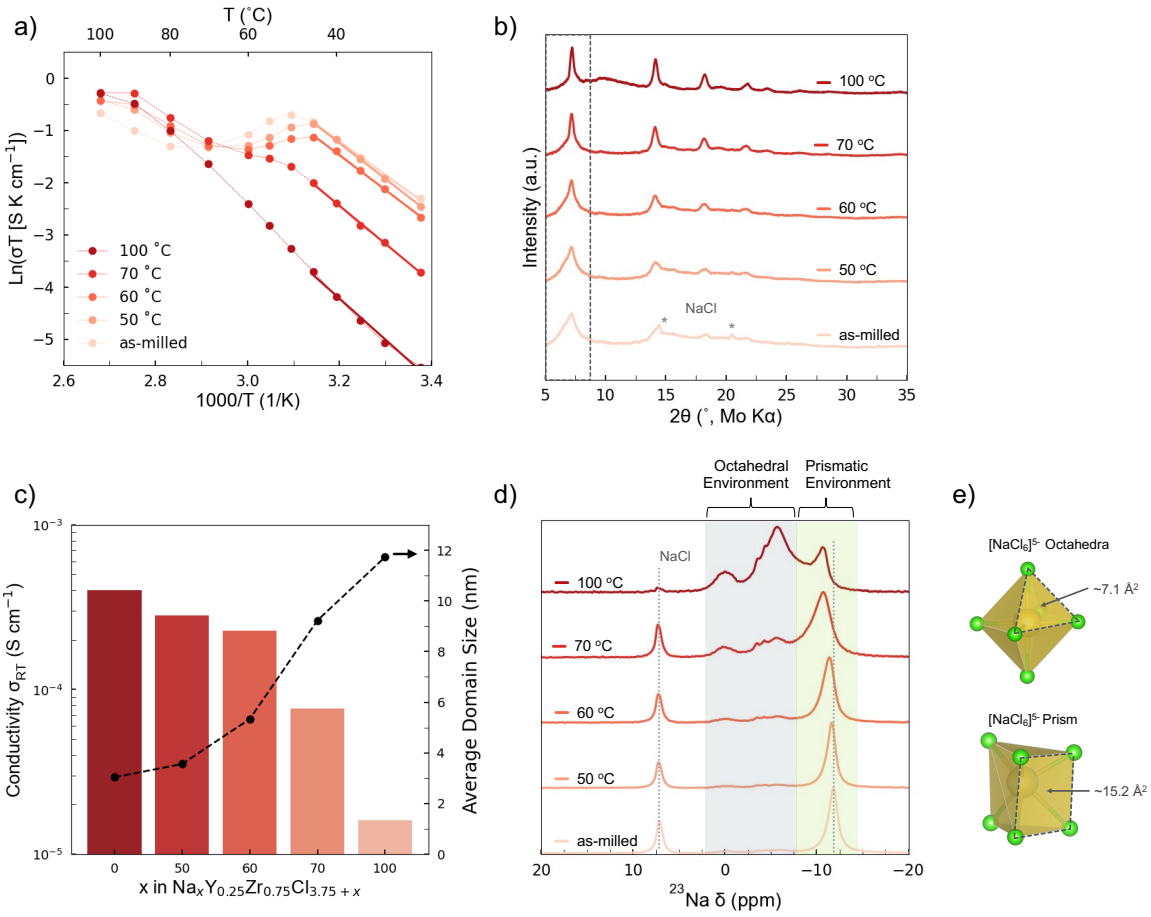

Figure 3. a) Arrhenius plot for the NYZC-0.625 samples recovered after heat treatment at 50, 60, 70, and 100 °C. b) XRD patterns of $Na_xY_{0.25}Zr_{0.75}Cl_{3.75+x}$ (x = 0.625) samples recovered after heat treatment. c) Relationship between average domain size and ionic conductivity in $Na_{0.625}Y_{0.25}Zr_{0.75}Cl_{4.375}$ (x = 0.625) heat-treated samples. d) ^{23}Na ss-NMR spectra recorded on $Na_{0.625}Y_{0.25}Zr_{0.75}Cl_{4.375}$ (x = 0.625) heat-treated samples. e) Schematic depicting $[NaCl_6]^{5-}$ octahedral and prismatic environments.

Electrochemical Testing. To examine the effect of Na-deficiency on the electrochemical performance of a solid-state battery, a cell using the Na-deficient NYZC-0.625 phase as a catholyte was compared to one comprising the stoichiometric NYZC-2.25 phase (**Figure 4a**). At room temperature and a 0.1 C current rate (where 1 C = 120 mA g^{-1} and 71 μA cm^{-2}), the Na-deficient catholyte cell exhibited a higher first cycle Coulombic efficiency (CE) of ~95% compared to ~92% for $Na_{2.25}Y_{0.25}Zr_{0.75}Cl_6$. Moreover, the Na-deficient phase delivered higher initial charge and discharge capacities compared to those of stoichiometric $Na_{2.25}Y_{0.25}Zr_{0.75}Cl_6$ (**Figure 4a**). These higher capacity values can be attributed to the higher ionic conductivity and more favorable SE

deformability due to the low crystallinity nature of the sample, which leads to an improved contact between cathode and SE particles, and a better of utilization of the cathode active material in the composite.[37]

Rate capability tests using a sequence of 0.1, 0.2, 0.5, 1, and 0.1 C current rates also reveal that the Na-deficient phase exhibits superior electrochemical performance at high current densities (**Figure 4b** and **4c**). The performances of the two catholytes, NYZC-0.625 and NYZC-2.25, show little difference at lower C-rates (0.1 and 0.2 C). It should be noted that although the normalized capacities are similar, the cathode utilization is lower in the case of the stoichiometric phase, as previously indicated. At higher current rates (0.5 and 1 C), the difference in the performance of Na-deficient and stoichiometric compositions become obvious. Na-deficient composition enables the cathode to deliver nearly 80% (~97 mAh g^{-1}) and 60% (~70 mAh g^{-1}) of its initial discharge capacity at 0.5 C and 1 C, respectively, while the values are only 70% (71 mAh g^{-1}) and 40% (43 mAh g^{-1}) when using stoichiometric NYZC-2.25 system. The low ionic conductivity of the stoichiometric composition manifests as greater overpotential, especially at high current rates, indicating a higher overall resistivity of the cathode composite and a lower utilization of its capacity.

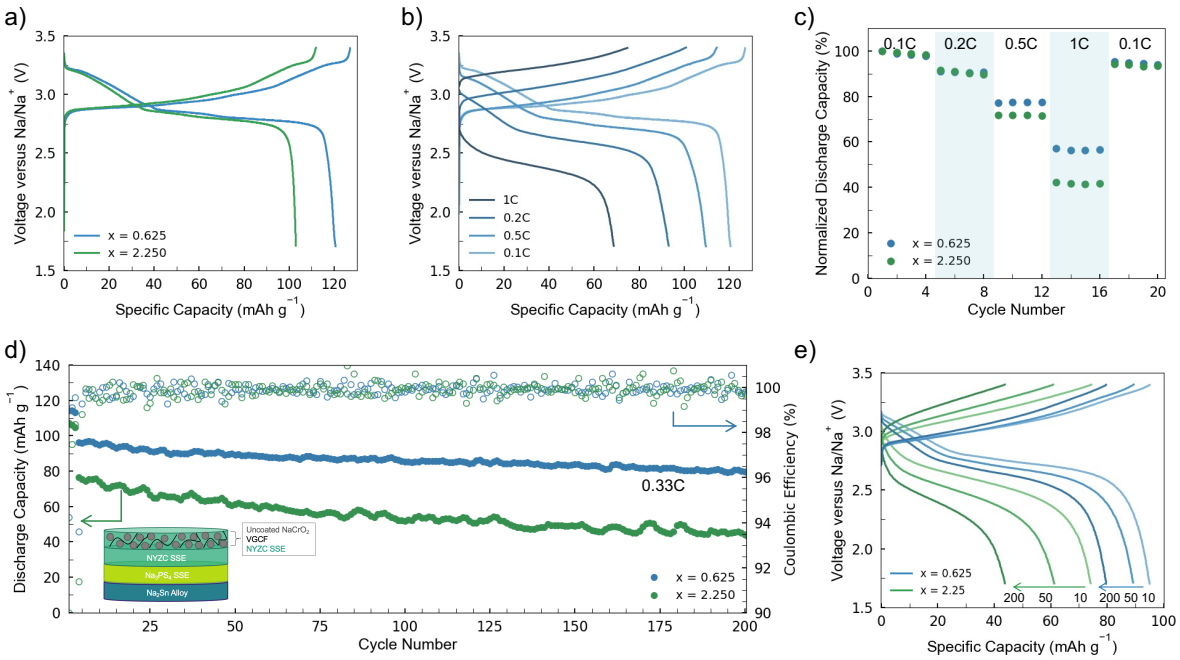

Figure 4. a) First cycle voltage profile of the Na-deficient NYZC-0.625 phase (x = 0.625) and the stoichiometric NYZC-2.25 (2.25) phase at 0.1 C rate. b) Voltage profiles at varying C-rates for $Na_xY_{0.25}Zr_{0.75}Cl_{3.75+x}$ (x = 0.625) material. c) Rate study comparison for both NYZC-0.625 and NYZC-2.25 materials. d) Extended cell cycling at 0.33C rate for both NYZC-0.625 and NYZC-2.25 materials. e) Voltage profiles corresponding to the extending cycling data. Cycles 10, 50, and 200 are indicated for both samples.

Beyond the rate study, long-term cycling at 0.33 C also shows that the Na-deficient NYZC-0.625 composition leads to a better performance with an average CE of 99.8% and a capacity retention of 83.3% is achieved after 200 cycles (**Figure 4d**). Conversely, an average CE of 99.6% and a capacity retention of 58.2% are observed after 200 cycles for the stoichiometric NYZC-2.25. Previously, the oxidative stability window for NYZC-2.25 was reported to be upwards of 3.8 V vs. Na/Na^+.[4] The electrochemical stability window for the Na-deficient NYZC-0.625 composition was measured (**Figure S2**) and found to be similar to that of the stoichiometric phase. Moreover, there is a four order of magnitude difference between the ionic and electronic conductivities of the Na-deficient phase (**Figure S3)**, indicating the Na-deficient composition remains a good solid electrolyte. While both materials are expected to be both chemically and electrochemically stable

under these cycling conditions the Na-deficient phase possessed a higher ionic conductivity, helping to improve the performance of Na-ASSBs at room temperature.

From the material point of view, the $Na_xY_{0.25}Zr_{0.75}Cl_{3.75+x}$ ($0.25 \leq x \leq 0.875$) SEs investigated in this study can be classified as glass-ceramics. Traditionally, melt quenching has been utilized to induce the vitreous state and has been the primary method for synthesizing various oxide, chalcogenide, and halide glasses or glass-ceramics.[38] While oxide and chalcogenide glasses have long been studied as potential solid electrolyte candidates, their ionic conductivities at ambient temperature are rather low, making them impractical for use in battery applications. On the other hand, the development of halide glasses lags their oxide and chalcogenide counterparts due to their highly hygroscopic nature and high crystallization rates during cooling.[38] However, recent developments of inert operational environments, e.g., gloveboxes, and mechanochemical ball-milling have helped to obtain structurally similar glassy or amorphous states without the need for rapidly cooling a melt.[39] In 1980, Ravaine conducted a systematic study on the influence of the networking forming cation, modifier cation, and anion on the conductivity of mobile ions in the glass matrix, where it was shown that with the same networking forming and modifier cations, the Na^+ conductivity in sulfide glasses was two to three orders of magnitude higher than in oxides glasses.[40] This observation was explained by the lower interaction energy between Na^+ and the sulfide network, which is a consequence of the lower charge density of S^{2-} compared to O^{2-}. In chloride glass, the charge density of Cl^- is even lower than S^{2-}, which could be one of the factors contributing to the high ionic conductivity of the N_xYZC_x SEs studied in this work.

Recent studies on halide-based SEs focus on optimizing the nature, size, and charge of the aliovalent substituent to control the vacancy density and the size of bottleneck on the diffusion pathway to obtain an optimum ionic conductivity value.[23] In this study, we introduce the prospect of using chloride glass-ceramics as promising SEs for Na-ASSBs. Unlike oxide and chalcogenide glasses, the chloride N_xYZC_x glass-ceramics exhibited higher ionic conductivity in the amorphous state rather than the crystallized phase. The results of this work may open a new research direction in the community and revive the use of glass and glass-ceramic solid electrolytes, whose ionic conductivity depends greatly on the nature and the ratio of the network forming and structural modifiers

In this study, a new approach for designing highly conductive chloride-based Na^+ ion conductors with low crystallinity was introduced. The use of ball-milling synthesis and Na-deficiency results in synergistic effects on the local structure of Na, crystallinity, and enhances the ionic conductivity of the prepared samples. The as-milled samples obtained from this synthesis approach had their Na^+ ions residing preferentially in prismatic environments, which possibly possess a lower activation energy for Na^+ hopping. Furthermore, the low NaCl molar percentage, combined with ball-milling synthesis, resulted in the formation of samples with low crystallinity, which likely exhibit more free volume and higher number of Na vacancies as compared to the stoichiometric NYZC-2.25 system, both of which are necessary for achieving high ionic conductivity. Such factors impact both the structure and the Na^+ mobility, which were evidenced by XRD, ss-NMR, and EIS measurements. The increased ionic conductivity of the Na-deficient compositions led to an improvement in the performance of Na-ASSBs, especially at high current rates and during long-term cycling tests. Interestingly, the Na-deficient compositions exhibited non-linear Arrhenius relationship at high temperatures, which is due to crystallization of the phase and the redistribution of Na among local prismatic and octahedral environments within the structure. This work provides insights into glass-ceramic chlorides and demonstrates new solid electrolyte design principles that could lead to a paradigm shift in the development of future Li^+ and Na^+ conductors for high-performance room temperature ASSBs.

Acknowledgements

P.R. acknowledges Corning Inc. for having supported his Ph.D. research through the Corning Glass Age Scholarship. Funding to support this work was provided by the National Science Foundation through the Partnerships for Innovation (PFI) grant No. 2044465. Characterization work was performed in part at the San Diego Nanotechnology Infrastructure (SDNI), a member of the National Nanotechnology Coordinated Infrastructure, which is supported by the National Science Foundation under Grant ECCS-1542148. This work also made use of the shared facilities of the UC Santa Barbara MRSEC (Grant DMR 1720256), a member of the Materials Research Facilities Network (http://www.mrfn.org), and the computational facilities administered by the Center for Scientific Computing at the CNSI and MRL (an NSF MRSEC; Grants CNS 1725797 and DMR 1720256).

References

1. Yang, H.-L. *et al.* Progress and Challenges for All-Solid-State Sodium Batteries. *Advanced Energy and Sustainability Research* **2**, 2000057 (2021).
2. Hirsh, H. S. *et al.* Sodium-Ion Batteries Paving the Way for Grid Energy Storage. *Advanced Energy Materials* **10**, 2001274 (2020).
3. Sayahpour, B. *et al.* Perspective: Design of cathode materials for sustainable sodium-ion batteries. *MRS Energy & Sustainability* (2022) doi:10.1557/s43581-022-00029-9.
4. Wu, E. A. *et al.* A stable cathode-solid electrolyte composite for high-voltage, long-cycle-life solid-state sodium-ion batteries. *Nat Commun* **12**, 1256 (2021).
5. Kato, Y. *et al.* High-power all-solid-state batteries using sulfide superionic conductors. *Nat Energy* **1**, 1–7 (2016).
6. Yamane, H. *et al.* Crystal structure of a superionic conductor, Li7P3S11. *Solid State Ionics* **178**, 1163–1167 (2007).
7. Kamaya, N. *et al.* A lithium superionic conductor. *Nature Materials* **10**, 682–686 (2011).
8. Hayashi, A., Noi, K., Sakuda, A. & Tatsumisago, M. Superionic glass-ceramic electrolytes for room-temperature rechargeable sodium batteries. *Nature Communications* **3**, 856 (2012).
9. Song, S., Duong, H. M., Korsunsky, A. M., Hu, N. & Lu, L. A Na+ Superionic Conductor for Room-Temperature Sodium Batteries. *Scientific Reports* **6**, 32330 (2016).
10. Hayashi, A. *et al.* A sodium-ion sulfide solid electrolyte with unprecedented conductivity at room temperature. *Nat Commun* **10**, 5266 (2019).
11. Liu, Y. *et al.* Development of the cold sintering process and its application in solid-state lithium batteries. *Journal of Power Sources* **393**, 193–203 (2018).

12. Ke, X., Wang, Y., Ren, G. & Yuan, C. Towards rational mechanical design of inorganic solid electrolytes for all-solid-state lithium ion batteries. *Energy Storage Materials* **26**, 313–324 (2020).
13. Wenzel, S. *et al.* Interfacial Reactivity Benchmarking of the Sodium Ion Conductors Na3PS4 and Sodium β-Alumina for Protected Sodium Metal Anodes and Sodium All-Solid-State Batteries. *ACS Appl. Mater. Interfaces* **8**, 28216–28224 (2016).
14. Culver, S. P., Koerver, R., Zeier, W. G. & Janek, J. On the Functionality of Coatings for Cathode Active Materials in Thiophosphate-Based All-Solid-State Batteries. *Advanced Energy Materials* **9**, 1900626 (2019).
15. Han, Y. *et al.* Single- or Poly-Crystalline Ni-Rich Layered Cathode, Sulfide or Halide Solid Electrolyte: Which Will be the Winners for All-Solid-State Batteries? *Advanced Energy Materials* **11**, 2100126 (2021).
16. Asano, T. *et al.* Solid Halide Electrolytes with High Lithium-Ion Conductivity for Application in 4 V Class Bulk-Type All-Solid-State Batteries. *Advanced Materials* **30**, 1803075 (2018).
17. Li, X. *et al.* Air-stable Li3InCl6 electrolyte with high voltage compatibility for all-solid-state batteries. *Energy Environ. Sci.* **12**, 2665–2671 (2019).
18. Park, K.-H. *et al.* High-Voltage Superionic Halide Solid Electrolytes for All-Solid-State Li-Ion Batteries. *ACS Energy Lett.* **5**, 533–539 (2020).
19. Kwak, H. *et al.* New Cost-Effective Halide Solid Electrolytes for All-Solid-State Batteries: Mechanochemically Prepared Fe3+-Substituted Li2ZrCl6. *Advanced Energy Materials* **11**, 2003190 (2021).

20. Kim, S. Y. *et al.* Lithium Ytterbium-Based Halide Solid Electrolytes for High Voltage All-Solid-State Batteries. *ACS Materials Lett.* 930–938 (2021) doi:10.1021/acsmaterialslett.1c00142.

21. Zhou, L. *et al.* High areal capacity, long cycle life 4 V ceramic all-solid-state Li-ion batteries enabled by chloride solid electrolytes. *Nat Energy* 1–11 (2022) doi:10.1038/s41560-021-00952-0.

22. Sebti, E. *et al.* Stacking Faults Assist Lithium-Ion Conduction in a Halide-Based Superionic Conductor. *J. Am. Chem. Soc.* (2022) doi:10.1021/jacs.1c11335.

23. Schlem, R., Banik, A., Eckardt, M., Zobel, M. & Zeier, W. G. Na3–xEr1–xZrxCl6—A Halide-Based Fast Sodium-Ion Conductor with Vacancy-Driven Ionic Transport. *ACS Appl. Energy Mater.* **3**, 10164–10173 (2020).

24. Liang, J. *et al.* Site-Occupation-Tuned Superionic LixScCl3+xHalide Solid Electrolytes for All-Solid-State Batteries. *J. Am. Chem. Soc.* **142**, 7012–7022 (2020).

25. Park, D. *et al.* Materials design of sodium chloride solid electrolytes Na3MCl6 for all-solid-state sodium-ion batteries. *J. Mater. Chem. A* **9**, 23037–23045 (2021).

26. Qie, Y. *et al.* Yttrium–Sodium Halides as Promising Solid-State Electrolytes with High Ionic Conductivity and Stability for Na-Ion Batteries. *J. Phys. Chem. Lett.* 8 (2020).

27. Zhang, K. & Jin, Z. Halogen-enabled rechargeable batteries: Current advances and future perspectives. *Energy Storage Materials* **45**, 332–369 (2022).

28. Kwak, H. *et al.* Na2ZrCl6 enabling highly stable 3 V all-solid-state Na-ion batteries. *Energy Storage Materials* **37**, 47–54 (2021).

29. Zhang, Z. *et al.* Targeting Superionic Conductivity by Turning on Anion Rotation at Room Temperature in Fast Ion Conductors. *Matter* **2**, 1667–1684 (2020).

30. Harris, R. K. & Nesbitt, G. J. Cross polarization for quadrupolar nuclei—Proton to sodium-23. *Journal of Magnetic Resonance (1969)* **78**, 245–256 (1988).
31. Sebti, E. *et al.* Synthetic control of structure and conduction properties in Na–Y–Zr–Cl solid electrolytes. *Journal of Materials Chemistry A* **10**, 21565–21578 (2022).
32. Yabuuchi, N. *et al.* New O2/P2-type Li-Excess Layered Manganese Oxides as Promising Multi-Functional Electrode Materials for Rechargeable Li/Na Batteries. *Advanced Energy Materials* **4**, 1301453 (2014).
33. Nguyen, H. *et al.* Single-step synthesis of highly conductive Na3PS4 solid electrolyte for sodium all solid-state batteries. *Journal of Power Sources* **435**, 126623 (2019).
34. Bamford, D. *et al.* Ionic conductivity, glass transition, and local free volume in poly(ethylene oxide) electrolytes: Single and mixed ion conductors. *J. Chem. Phys.* **118**, 9420–9432 (2003).
35. Swenson, J. & Börjesson, L. Correlation between Free Volume and Ionic Conductivity in Fast Ion Conducting Glasses. *Phys. Rev. Lett.* **77**, 3569–3572 (1996).
36. Smith, J. G. & Siegel, D. J. Low-temperature paddlewheel effect in glassy solid electrolytes. *Nature Communications* **11**, 1483 (2020).
37. Sakuda, A., Hayashi, A. & Tatsumisago, M. Sulfide Solid Electrolyte with Favorable Mechanical Property for All-Solid-State Lithium Battery. *Sci Rep* **3**, 2261 (2013).
38. Poulain, M. Halide glasses. *Journal of Non-Crystalline Solids* **56**, 1–14 (1983).
39. Berbano, S. S., Seo, I., Bischoff, C. M., Schuller, K. E. & Martin, S. W. Formation and structure of Na2S+P2S5 amorphous materials prepared by melt-quenching and mechanical milling. *Journal of Non-Crystalline Solids* **358**, 93–98 (2012).
40. Ravaine, D. Glasses as solid electrolytes. *Journal of Non-Crystalline Solids* **38–39**, 353–358 (1980).